

# Numerical modelling of the hydrodynamics around the farm of Wave Activated Bodies (WAB)

E. Angelelli<sup>1</sup>, B. Zanuttigh<sup>2</sup> and J.P. Kofoed<sup>3</sup>

<sup>1</sup> Civil, Environmental and Materials Engineering DICAM,  
University of Bologna,  
Viale Risorgimento 2, 40136 Bologna, Italy  
E-mail: elisa.angelelli4@unibo.it

<sup>2</sup> Civil, Environmental and Materials Engineering DICAM,  
University of Bologna,  
Viale Risorgimento 2, 40136 Bologna, Italy  
E-mail: barbara.zanuttigh@unibo.it

<sup>3</sup> Department of Civil Engineering,  
University of Aalborg,  
Sohngaardsholmsvej 57, 9000 Aalborg, Denmark  
E-mail: jpk@civil.aau.dk

## Abstract

The aim of this research is to develop a numerical modelling approach able to provide design criteria for the optimization of the layout of a farm of Wave Energy Converters (WECs).

The numerical model MIKE 21BW is calibrated against the experimental results obtained in Aalborg wave tank for a farm of floating WECs. The WECs under exam belong to the Wave Activated Body type. The calibrated model allows to tests more configurations at lower cost than physical models. Specifically, different mutual distance among the devices and their mutual alignment are examined to maximise the density of the devices and the distribution of residual wave energy and therefore energy production. Simulated and measured wave heights recorded by the many wave gauges placed in the basin are compared, as well as wave transmission and reflection induced by the devices.

A sensitivity analysis, i.e. the identification of the key model parameters to be tuned in order to optimise the comparison, is also carried out.

**Keywords:** DEXA, experiments, hydrodynamics, numerical simulation and calibration, transmission coefficient, wave energy converter, wave farm.

## 1. Introduction

In the literature there are many contributions dealing with the analysis of wave loads on WECs, usually

tested in a wave tank to jointly assess the power production and optimise the design, while investigation of WECs placed in farms is rather limited. Most of the investigations of WECs array deals with the influence of such installation on the littoral or vice versa on the estimated power conversion capacity based on a detailed wave and tidal climate and on the simplified assumption that each device produce a given energy absorption [1], [2].

The numerical methods adopted so far to model the wave field around WECs are essentially based on three different approaches.

The first approach is the traditional simplified modelling adopted for vessels and floating breakwaters, which is relative to the 2D case (indefinitely long structure with perpendicular wave attack) and is based on the hypothesis of irrotational flow. Available commercial codes as WAMIT, AQWA are based on the Boundary Element Method. These models are typically implemented for uniform bottom, linear waves and do not account for viscous dissipation, hypotheses which become less accurate if referred to shallow water conditions [1].

The second approach consists of 2D or 3D models typically developed to assess the impact on the littoral of wind farms and then applied also to wave farms where the piles or devices are represented through an equivalent bottom friction or percentage of wave energy absorption respectively [3]. These simulations are usually done for environmental impact assessment purposes and do not consider model calibration.

The third approach uses 2DV and 3D RANS-VOF models to represent velocities and pressure around

floating bodies. Simulations are usually always calibrated against experimental data in wave flume or tank. The first applications were performed on single and multiple floating breakwaters but fixed [4]; more advanced research proposed 3D models combined with the external solution of the motion equation and iteratively solved. In this way it is possible to reproduce the presence of PTO or moorings by means of the external forces applied to the WEC [5].

A recent work [6] applied a 2D Boussinesq model to reproduce the hydrodynamics around a Wave Dragon, based on the experimental results obtained in wave tank. The wave reflection and transmission from the WEC were modelled by using porous layers with calibrated coefficients around the device.

The numerical modelling approach presented in this paper builds on this last work. In this case, multiple WECs of the Wave Activated Body type are analysed within a staggered wave farm. Synthetic descriptions of the device and of the numerical tool are provided in Section 2 and 3 respectively. The details of the experimental and numerical set-up are reported in Section 4. The most relevant results, such as incident wave energy, wave heights in the basin, wave reflection and transmission induced by the devices are compared in Section 5. Once the model is calibrated, two additional configurations with aligned devices and staggered devices but reduced gap width are examined in Section 6. Conclusions about the approach and the design layout of the wave farm are finally drawn in Section 7.

## 2. Device Description

The floating WEC under investigation is called DEXA ([www.dexawave.com](http://www.dexawave.com)). It consists of two rigid pontoons with a hinge in between, which allows each pontoon to pivot in relation to the other (see Fig. 1). The draft is such that at rest the free water surface passes in correspondence of the axis of the four buoyant cylinders. The Power Take-Off (PTO) system consists of a low pressure power transmission technology [7].



Figure 1: DEXA Concept ([www.dexawave.com](http://www.dexawave.com)).

For the purpose of this analysis, 1:60 scale models in Froude similitude were tested. Each model is 0.96 m long (dimension in the following indicated with  $l$ ) and 0.38 m wide (dimension indicated with  $b$ ). As for the

prototype, the floating model is composed by two parts connected with an elastic resistant strip.

The model was moored with a “spread type”, i.e. using four steel chains (each 1.5 m long) fixed to the bottom with heavy anchors (3 kg each) and linked to the device at the fairlead point in the middle of the legs.

Three identical models were available to carry out experiments on the effects induced by a wave farm (see Fig. 2). Since the main target is the evaluation of the hydrodynamics induced by the farm, these models do not carry PTO systems or measurement instrumentations on board.

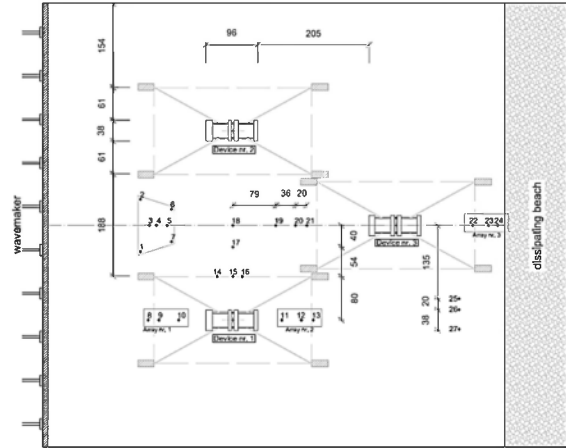


Figure 2: Wave farm configuration, distances are in cm.

## 3. Numerical model description

The numerical simulations have been carried out using the software MIKE 21 BW, developed by DHI [8]. MIKE 21 is a modelling system for 2D free-surface flows, such as e.g. estuaries, coastal waters and seas. MIKE 21 BW, i.e. the Boussinesq Wave module, is the model for calculation and analysis of short- and long-period waves in ports and coastal areas.

This model is based on the numerical solution of the enhanced Boussinesq equations formulated by Madsen and Sørensen [9] and their updates related to the wave breaking and moving shoreline [10]. MIKE 21 BW is capable of reproducing the combined effects of important wave phenomena, such as shoaling, refraction, diffraction, partial reflection and transmission from obstacles and internal wave generation (including directional spreading).

In particular to represent the hydrodynamics induced by a WEC farm the 2DH BW Module (two horizontal space co-ordinates, with rectangular grid) was chosen.

## 4. Description of the setups

This section describes both the numerical and the experimental set-up, since the laboratory results [11] were used to calibrate the numerical simulation.

### 4.1 Wave States

Previous physical tests on DEXA models showed that wave transmission coefficient  $K_T$  and efficiency tend to decrease and increase respectively with

increasing the dimensionless length  $l/L_p$ , where  $L_p$  is the peak wave length [11]. For the purpose of this analysis, eight wave states (WSs) have been considered. These WSs correspond to 3D Jonswap irregular non-breaking waves (see Tab. 1). Since Zanuttigh et al. [11] highlights that the installation water depth and the wave steepness do not strongly affect the  $K_T$ , the selected WSs were performed all on the water depth  $h_f=0.30$  m. All the water condition represent intermediate condition, where  $1/20 < h_{max}/L_o < 1/2$ .

WS	$H_s$ [m]	$T_p$ [s]	$L_p$ [m]	$l/L_p$
1	3.00	5.7	49.7	1.20
2	3.00	6.5	62.8	1.00
3	3.00	7.8	83.3	0.75
4	3.00	10.6	125.7	0.50
5	4.00	7.8	83.3	0.75
6	4.00	10.6	125.7	0.50
7	5.00	7.8	83.3	0.75
8	5.00	10.6	125.7	0.50

**Table 1:** Selected Wave States for the calibration, where  $H_s$  is the significant incident wave height,  $T_p$  is the peak wave period,  $L_p$  is the peak wave length and  $l$  is the device length; values are in full scale.

#### 4.2 Laboratory wave farm

Figure 2 shows the tested wave farm layout. In particular it consists of a staggered configuration with two models (device nr. 1 and 2) deployed along the first farm line (towards the wave-maker), with a 3.10 m wide central gap in between (8b). In order to simulate the presence of the second farm line, a third model was placed just behind the gap.

The physical tests were performed in the directional deep wave basin of the Hydraulics and Coastal Engineering Laboratory at Aalborg University, DK. The basin is 15.7 m long (in waves direction), 8.5 m wide and 1.5 m as maximum deep. To reduce the reflection from the basin, the sidewalls are made of crates and a 1:4 dissipative beach, made of concrete and gravel with  $D_{50}=5$  cm, is placed opposite to the wave maker.

#### 4.3 Numerical wave farm and parameters

The numerical bathymetry exactly reproduced the basin and the beach. Bottom friction was included by means of a constant Manning number of  $40 \text{ m}^{1/3}/\text{s}$  for the concrete bottom and of  $30 \text{ m}^{1/3}/\text{s}$  for the devices. A varying Manning number between 40 and  $20 \text{ m}^{1/3}/\text{s}$  was adopted for the beach.

The three floating devices were reproduced as porous layers, in order to simulate wave transmission and reflection through them. The selection of the value to be attributed to the porous layers, i.e. the so called porous factor, has been derived from an iterative procedure. The internal Toolbox of MIKE 21 “Wave reflection coefficient” allows to obtain the value of this factor depending on the water depth, the wave conditions, the width and permeability of the layer and on the typical diameter of the stones. The value can be

selected to match the measured reflection and transmission coefficients.

The porous factor proved to be the key design and calibration parameter. After several attempts, in order to optimise the representation of wave transmission, a porous factor of 0.90 has been selected.

To assure full wave absorption behind the numerical wave-maker a sponge layer of 50 cells has been created. The assigned sponge values are obtained, as for the porosity factor, through an internal Toolbox. The set-up of the sponge layer fulfilled the provided guidelines [8], for instance: the sponge layer width should be one/two times the wave length corresponding to the most energetic waves; sponge layers should be at least 20 lines wide (but 50 are suggested); to minimise reflections, the values of the sponge layer coefficients increase smoothly towards the boundary/land.

In the tested configuration  $h_{max}/L_o$  is often lower than 0.22, hence the classical Boussinesq formulation (deep water terms excluded) has been chosen. For the smallest wave periods (i.e.  $h_{max}/L_o$  0.40) the comparison among simulations run both with the classical and with the enhanced Boussinesq equations show in the latter case lower incident wave energy spectra and lower wave heights along the basin. Moreover the model requires more CPU time, therefore all the results here presented were obtained from simulations run with the classical formulation.

In order to guarantee the numerical stability of the simulation, a high-resolution in both space and time was selected. The grid spacing in both cross-shore (i.e. direction of wave propagation) and long-shore direction was equal to 0.05 m. The minimum wave period (i.e.  $T_p=0.74\text{s}$ ) was resolved by more than 35 time steps (i.e.  $T_{min}/3$ ) since the moving shoreline was included. Therefore the calculation time step of 0.01s was chosen.

The chosen space and time discretization fulfil the Courant criterion, i.e.  $CR < 1.00$ . Furthermore to be sure that an efficient space and time model resolution was selected, the suggested values from MIKE 21 BW Model Setup Planner, included in the Online Help, were also checked.

#### 4.4 Measurements

The hydrodynamic measurements were performed by using in the physical basin a total number of 27 resistive Wave Gauges (WGs), which give the instantaneous value of the surface elevation. All data were simultaneously acquired at the sample frequency of 20 Hz by means of WaveLab, a software developed by Aalborg University [12]. This software allowed also to automatically perform the calibration procedure.

Figure 2 shows six groups of three WGs, which are necessary to calculate the incident wave height ( $H_I$ ) and the reflected one ( $H_R$ ). In particular, data processing presented in the next Section will refer to WGs nr 8-10 placed in front of the device nr. 1, WGs nr 11-13, placed behind the same device and WGs 22-24 placed behind the device nr. 3.



In the numerical simulation -a part from the 2D maps- the results are extracted in time in correspondence of the same 27 positions to evaluate the wave height and the wave transmission, in the time and frequency domain.

Since the calculation time step is 0.01s, the output was post processed to avoid different sample frequency between the lab and the numerical model.

## 5. Calibration analysis

In order to tune the numerical model, the values of the setup parameters have been calibrated based on the comparison between the numerical outputs and the physical significant wave heights  $H_S$  and  $K_T$  values.

### 5.1 Wave Generation and Energy comparison

Measured and simulated wave energy spectra were compared based on the frequency analysis domain at the groups of three aligned WGs [13] in front the wave maker and along the basin.

As regards wave generation, the numerical model is able to predict the incident wave energy at the WGs 8-9-10 (see Fig. 3a), being the energy difference at the peak frequency on an average of the 3%. The worst case, leading to a difference up to the 18%, corresponds to the lower WS, i.e. WS nr. 2, where problems in generation may have occurred due to wave-maker limitations [11].

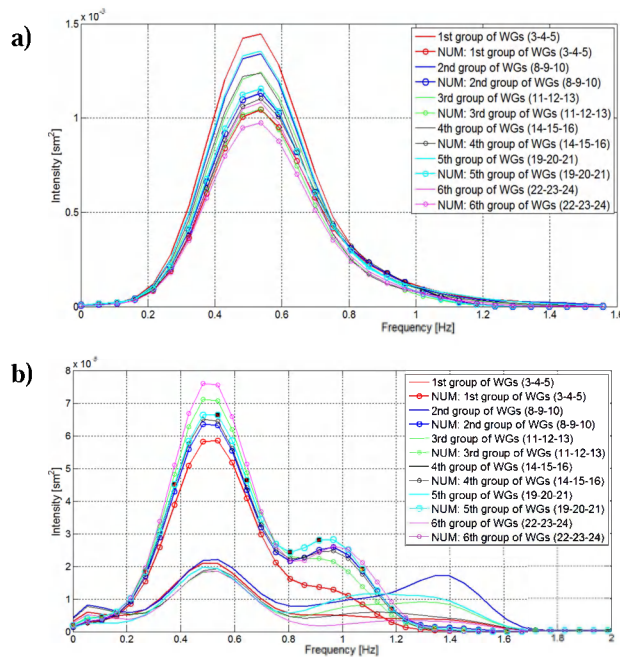


Figure 3: Lab and numerical conditions of the incident (a) and reflected (b) energy spectrum for the WS8.

The validity of the energy comparison is also proven by the 3D - BDM analysis carried out on the first 7 WGs. This method allows to highlight that the directional spreading is higher in the laboratory than in the numerical simulation.

Regarding the reflected wave energy, instead, the model overestimates the lab values at least of 2.5 times (see Fig. 3b).

### 5.2 Wave Height

The values of the numerical  $H_S$  along the basin are close to the experimental ones with the exception of the WGs within the gap (see Fig. 4). The reason of the differences in the gap is due to the device motion, since in the numerical simulation the device is modelled as a fixed body (a porous pile with rectangular section). Indeed, if we compare for brevity the long-shore distribution of the wave heights across the gap (see Fig. 5), the wave height in the lab tends to decrease from the centre of the gap towards the device (i.e. from WG 18 to WG 15) while in the simulation instead the trend seems to be constant.

Furthermore also the different spreading, seen in the paragraph 5.1, leads to a different wave height distribution in the wake of the devices.

Besides, it can be observed that the numerical wave maker is more stable than the wave-maker in the laboratory [11]: in fact it is able to reproduce the same  $H_T$  by changing  $T_p$  also for the less energetic WSs (see WSs 1-2 in the Fig. 4).

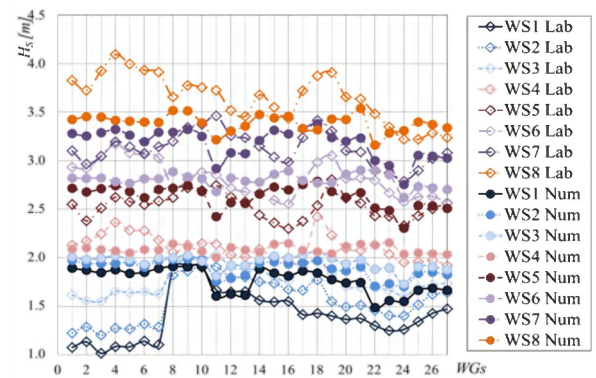


Figure 4: Comparison of the  $H_S$  recorded in the 27 WGs placed along the basin. Values are in full scale.

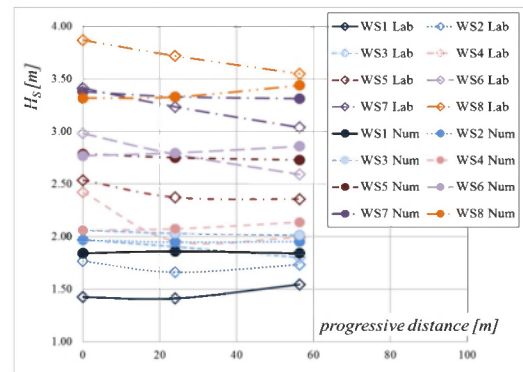


Figure 5:  $H_S$  in long-shore direction, where the zero is at the centre of the gap (WG 18). Values are full scale.

### 5.3 Wave Transmission

The values of  $K_T$  were calculated as the ratio between the wave height behind a device and the wave height at the wave-maker, both for the laboratory and the numerical tests.

Table 2 shows the comparison of  $K_T$ , where  $K_{Tf}$  is the  $K_T$  related to the front device (in the first line), and  $K_{Tb}$  is the  $K_T$  related to the back device (in the second line).

It is possible to note that the average values differ for less than the 3.5% for  $K_{Tf}$  and 7% for  $K_{Tb}$ . The higher differences are related to the back device due to a different wave height distribution along the gap of the first line, i.e. different representation in the model of the mutual interaction among the devices and different wake effects acting on this third device.

WS	$K_{Tf,LAB}$	$K_{Tf,NUM}$	$K_{Tb,LAB}$	$K_{Tb,NUM}$
1	0.88	0.82	0.68	0.82
2	0.96	0.90	0.77	0.86
3	0.97	0.94	0.83	0.92
4	0.97	0.97	0.95	0.96
5	0.97	0.93	0.89	0.90
6	0.97	0.96	0.94	0.94
7	0.99	0.92	0.86	0.89
8	0.96	0.95	0.90	0.92

Table 2:  $K_T$  for the lab tests and the numerical simulations.

#### 5.4 Wave Reflection

The reflection coefficient  $K_R$  is defined as the ratio between the reflected and the incident wave height in front of a device. Table 3 reports the results for the front device as  $K_{Rf}$  (derived from the WGs 8-9-10) and for the back device as  $K_{Rb}$  (derived from the WGs 19-20-21).

From the table it is seen that the  $K_{R,LAB}$  is in the range 16-34%,  $K_{R,NUM}$  instead varies in a wider range 27-70%. The much greater differences in the values of  $K_R$  than in the values of  $K_T$  can be related to a different representation of the dissipation induced by the beach. These differences may decrease by adding a porosity layer in the numerical beach. Of course the same reasons for discrepancy stated above in paragraph 5.3 (i.e. the device interaction in the gap and the different motion of the devices) still apply.

WS	$K_{Rf,LAB}$	$K_{Rf,NUM}$	$K_{Rb,LAB}$	$K_{Rb,NUM}$
1	0.32	0.53	0.34	0.70
2	0.28	0.41	0.28	0.48
3	0.23	0.39	0.21	0.44
4	0.18	0.39	0.17	0.39
5	0.23	0.35	0.20	0.39
6	0.18	0.38	0.16	0.38
7	0.25	0.32	0.22	0.36
8	0.19	0.27	0.17	0.28

Table 3:  $K_R$  for the lab tests and the numerical simulations.

## 6. Additional numerical configuration

Once the accuracy and the limitations of the software are well-known, it is possible to extend the physical database at lower cost.

Two design parameters of the farm layout have been selected so far: the alignment and the distance between the devices. In order to analyse both the influence of a change in wave height and wave period the numerical

tests were carried out for WSs 4-5-7. The main results are reported below.

### 6.1 Alignment

The first new configuration consists of a different placement of the devices in the basic module, by changing from a three staggered devices to a module with four aligned devices.

The main consequences are a slight decrease of the  $K_T$  of the back devices (see Tab. 4) and of the wave heights recorded at the last WGs 25-27 (in the back of the new device). It is indeed expected that the presence of a second device in the last line should affect only the results in the rear part.

WS	$K_{Tb,NUM 3 DEXA}$	$K_{Tb,NUM 4 DEXA}$
4	0.96	0.94
5	0.90	0.88
7	0.89	0.86

Table 4:  $K_T$  for the numerical simulations: with 3 DEXA in a staggered module, and with 4 DEXA in an aligned module.

### 6.2 Mutual Distances

The further analysis is related to the influence of the gap width using the staggered configuration. The gap width can be a design parameter able to optimize the combination of coastal protection and energy production. In fact the gap width reduction could increase the number of devices in the farm, i.e. the energy production, and at the same time could decrease the wave height behind the farm exploiting a constructive interaction between the devices in a same farm line.

In the simulation, the gap width has been decreased from 8b to 6b, leading, as expected, to modest changes in the  $H_I$  recorded in the gap (see Tab. 5).

WS	Gap width 8b		Gap width 6b	
	$H_{I, WG}$ 14-15-16	$H_{I, WG}$ 19-20-21	$H_{I, WG}$ 14-15-16	$H_{I, WG}$ 19-20-21
4	2.02	2.03	1.95	1.97
5	2.64	2.54	2.51	2.50
7	3.23	3.11	3.09	3.06

Table 6:  $H_I$  in the gap, in the staggered module, in the case of a gap width of 8b (left), and 6b (right).

### 6.3 Discussion of the numerical results

The results are qualitatively compared focusing on the hydrodynamic interaction among the devices, especially on the wake effect of the first line. The figures 6a,b,c report the disturbance coefficient  $K_D$ , defined as the ratio between the local  $H_S$  and the  $H_S$  recorded in front the wave-maker for the three configuration: three staggered devices with a gap width of 8b, four aligned devices with the same gap width of 8b, and a second staggered configuration with three devices with a smaller gap width of 6b.

The incident wave height in front of the back device depends on the wake of the front devices. In fact in figure 6b the back device is fully surrounded by the effects induced from its forward device, therefore it is predictable a reduction of its energy production. Figure

6c shows that the reduction of the gap width cause a constructive wave interaction in the gap of the first line, leading to an increasing of the wave height in front of the back device. Table 6 reports the range of  $K_D$  for the three analysed cases.

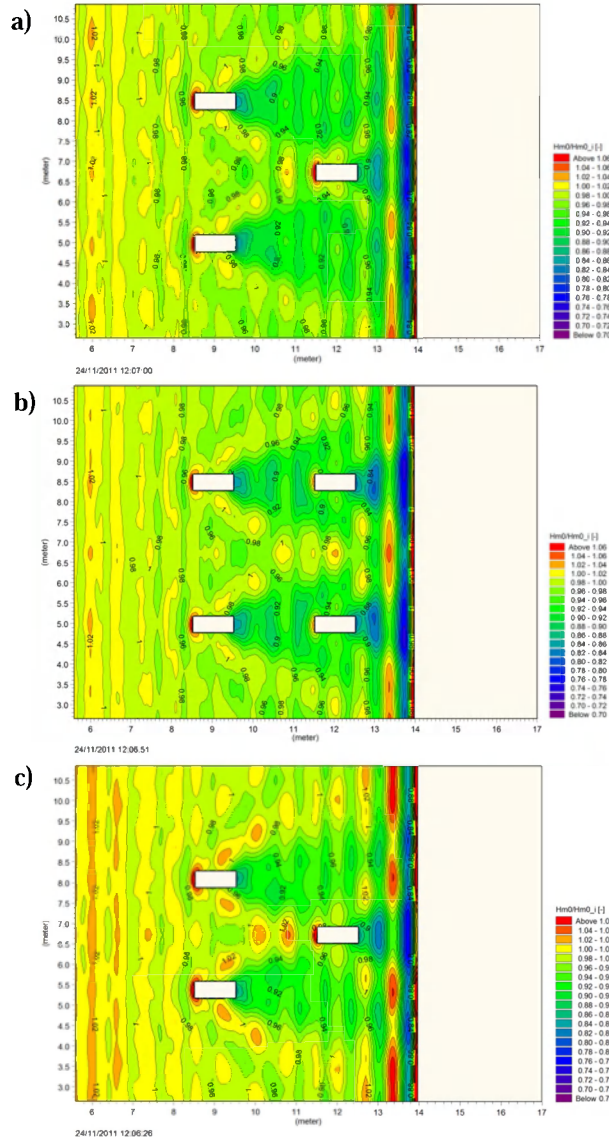


**Figure 6:**  $K_D$ , respectively: three staggered devices (gap width  $8b$ ), four aligned devices (same gap width) and three staggered devices with  $6b$  gap width.

Figure	Range of $K_D$ in the gap	Range of $K_D$ behind the back device
6a	0.98 – 0.90	0.94 – 0.86
6b	0.98 – 0.90	0.90 – 0.78
6c	1.02 – 0.90	0.92 – 0.82

**Table 6:** Range of  $K_D$  for the three analysed cases: 3 staggered devices (6a), 4 aligned devices (6b), and 3 staggered devices with a  $6b$  gap width (6c).

## 7. Conclusions

This paper presented for the first time the numerical modelling of a DEXA wave farm, with MIKE 21 BW, by DHI.

The devices have been reproduced as porous bodies and the simulations have been calibrated with a series of parameters based on physical tests, performed in the directional deep wave basin at Aalborg University, DK.

The calibrated model well reproduces the incident wave energy, the wave heights at the wave-maker and the wave transmission coefficient  $K_T$  induced by the devices. The values of  $K_T$  are particularly important, since they represent a measure of the residual wave energy to be re-converted by the rear devices.

The stability of the software with respect to the laboratory tests (i.e. the ability to reproduce the same incident wave height with changing the wave period) is considered a positive aspect for the validity of the simulation and its repeatability.

Reflected wave energy is overestimated by the model of about 2.5 times with respect to the measured values. A better representation –as further on-going work proves– may be achieved by using a porous layer in the numerical beach.

The model MIKE 21 BW is not able to accurately reproduce the wave field around the wave farm, especially in the space among the devices due to the impossibility to include the motion of the floating bodies.

Two additional configurations have been simulated and compared with the one tested in the laboratory.

When the staggered configuration is maintained, the decrease of the gap width leads to an overall greater incident wave height in front of the second line due to a constructive wave interaction in the gap.

When an aligned configuration is selected by keeping constant the gap width and the cross shore distance among the devices, the second line falls inside the wake of the first line and therefore the available residual wave energy is lower.

It is suggested thus to adopt a staggered layout and increase the density of the devices with decreasing the gap width but still allowing the moored devices to freely move.

The model was developed by DHI for full scale conditions, therefore it would be worthy to make additional simulations by repeating at prototype scale few of the tests performed at lab scale.

## Acknowledgements

The support of the European Commission through FP7 ENV2009-1, Contract 244104 - THESEUS project (“Innovative technologies for safer European coasts in a changing climate”), [www.theseusproject.eu](http://www.theseusproject.eu), and through FP7 OCEAN2011-1, Contract 288710 - MERMAID project (“Innovative Multi-purpose offshore platforms: planning, design and operation”), is gratefully acknowledged.

## References

- [1] J. Cruz, R. Sykes, P. Siddorn and R. Eatock Taylor. (2009): Wave Farm Design: Preliminary Studies on the Influences of Wave Climate, Array Layout and Farm

- Control. Proc. EWTEC 2009, Uppsala, Sweden, [http://www.see.ed.ac.uk/~shs/Wave%20Energy/EWTEC%202009/EWTEC%202009%20\(D\)/papers/218.pdf](http://www.see.ed.ac.uk/~shs/Wave%20Energy/EWTEC%202009/EWTEC%202009%20(D)/papers/218.pdf)
- [2] South West of England Regional Development Agency. (2006): Wave Hub Development and Design Phase Coastal Processes Study. [http://mhk.pnnl.gov/wiki/index.php/Wave\\_Hub\\_development\\_and\\_design\\_phase\\_coastal\\_processes](http://mhk.pnnl.gov/wiki/index.php/Wave_Hub_development_and_design_phase_coastal_processes)
  - [3] A. Palha, L. Mendes, J. F. Conceiç, A. Brito-Melo, A. Sarmiento. (2010): The impact of wave energy farms in the shoreline wave climate: Portuguese pilot zone case study using Pelamis energy wave devices. *Renewable Energy* 35 (2010) 62–77
  - [4] T. Koftis and P. Prinos. (2005): 2D-V Hydrodynamics of Double Floating Breakwaters. *Coastal Dynamics*
  - [5] E. Agamloh, A. Wallace and A. Von Jouanne. (2008): Application of fluid-structure interaction simulation of an ocean wave energy extraction device. *Renewable Energy*, Vol. 33, No. 4, pp. 748-757.
  - [6] C. Beels, P. Troch, K. De Visch, J.P. Kofoed and G. De Backer. (2010): Application of the time-dependent mild-slope equations for the simulation of wake effects in the lee of a farm of Wave Dragon wave energy converters, *Renewable Energy*, Volume 35, Issue 8, August 2010, Pages 1644-1661
  - [7] J.P. Kofoed. (2009): Hydraulic evaluation of the DEXA wave energy converter. DCE Contract Report No. 57. Dep. of Civil Eng., Aalborg University, Apr. 2009.
  - [8] DHI. (2008): MIKE21 Boussinesq waves module - User guide.
  - [9] P.A. Madsen and O.R. Sørensen. (1992): A new form of the Boussinesq equations with improved linear dispersion characteristics. Part 2: A slowly-varying Bathymetry. *Coastal Eng.* 18, 183-204.
  - [10] DHI. (2008): MIKE21 Boussinesq waves module - scientific documentation
  - [11] B. Zanuttigh, E. Angelelli, M. Castagnetti, J.P. Kofoed and L. Clausen. (2011): The Wave Field around DEXA Devices and Implications for Coastal Protection. *Control. Proc. 9th EWTEC 2011*, Southampton, UK
  - [12] Aalborg University. (2007): WaveLab3.33 Manual. homepage: <http://www.hydrosoft.civil.auc.dk/>
  - [13] E.P.D. Mansard and E.R. Funke. (1980): The measurement of incident and reflected spectra using a least squares method. *Proc. of the 17th Int. Conf. on Coastal Engineering*.